Engineering Fracture Mechanics Vol. 21, No. 2, pp. 405–421, 1985
Printed in the U.S.A.

0013–7944/85 $3.00 + .00

A COMPARISON OF METHODS FOR CALCULATING ENERGY RELEASE RATES

F. Z. LI, C. F. SHIH and A. NEEDLEMAN
Division of Engineering, Brown University, Providence, RI 02912 U.S.A.

Abstract—We compare two methods for calculating the energy released during quasi-static crack advance. One method is based on a surface integral (line integral in two dimensions) expression for the energy release rate, whereas the other method is based on a volume (area) integral representation. A concise derivation of the volume (area) integral expression is given using a virtual-work-type identity for Eshelby's energy momentum tensor. The finite-element implementation of the volume (area) integral formulation corresponds to the virtual crack extension method. Within the context of this formulation, we outline a procedure for calculating pointwise values of the energy release rate along a three-dimensional crack front. For illustrative purposes, numerical examples are presented for a fully plastic, plane strain, edge-cracked panel subject to combined tension and bending.

1. INTRODUCTION

A VERSATILE technique for determining the strength of the crack tip fields from finite-element solutions is by virtual crack extension. Parks has employed this technique for linear elastic solids [1] and deformation and incremental plasticity solids [2] and has discussed the extension to finite deformation plasticity [3]. Hellen [4] applied the technique to linear elastic problems, and more recently deLorenzi [5, 6] employed a similar method which was derived from somewhat more general considerations. Although the methods employed by Parks, Hellen and deLorenzi differ in detail, their methods are, in essence, techniques for determining the energy release rate from field solutions based on established energy variation concepts for deformation theory plasticity (nonlinear elasticity). In Refs. [1–4], a direct calculation of the variation in potential energy due to a virtual change of crack length was the basis for computing the energy release per unit area of crack advance (hereafter termed the energy release rate)—hence the name, virtual crack extension method. In [5] the energy release rate expression was obtained by mapping a cracked body into another cracked body of slightly different crack length.

As noted in Refs. [1–6], the greatest potential of the virtual crack extension technique is its obvious and straightforward application to the analyses of three-dimensional (3-D) cracked configurations. By appealing to the change in potential energy due to an arbitrary crack extension (in the plane of the crack) in the vicinity of the point s, the energy release rate $\mathcal{G}(s)$ can be defined pointwise along the crack front. To permit an accurate determination of $\mathcal{G}(s)$, the stresses and strains within the vicinity of the crack front must be known to within sufficient accuracy.

In [2], the virtual crack extension technique was applied to two-dimensional deformation plasticity finite-element solutions of deeply cracked plane strain bend specimens. It was noted that the energy release rate computed on the second, third, fourth and more remote rings of elements surrounding the crack tip had essentially the same values and that these values were also in close agreement with an independent evaluation of the energy release rate from the overall moment–rotation curve. Such behavior is indeed in accord with the continuum theory for a nonlinear elastic cracked body. However, the value of energy release rate determined from the first ring of elements (crack tip ring) was lower than the path-independent value by about 5, 18 and 7% in the elastic, contained plasticity and fully plastic regimes, respectively. The loss of accuracy from evaluations using the crack tip ring of elements was even greater for a center-cracked panel where the evaluated J integral was 30% too low in the fully plastic regime [2]. The loss of accuracy on the crack tip ring of elements does not pose any real difficulty in two-dimensional problems since by virtue of path independence, the energy release rate can be determined from remote rings of elements, where it can be evaluated accurately. However, this near-tip loss of accuracy has more serious consequences for three-dimensional crack analyses. In general, the determination of the pointwise energy release rate, $\mathcal{G}(s)$, along the crack

front requires values of field quantities (stresses, strains) in the first ring of elements surrounding the crack front.

The strength of the asymptotic two-dimensional crack tip fields can be characterized by the path-independent J integral of Rice [7], which can be evaluated from finite-element solutions using its line integral expression. It is tempting to extend such line integral methods to three-dimensional crack problems. Surface integral generalizations of the line integral expression for J [7] are available; see Eshelby [8, 9] and Budiansky and Rice [10]. However, it must be noted that these integrals are more appropriate for determining a global or "average" energy release rate than for obtaining a pointwise value along the crack front. The evaluation of the energy release rate pointwise along the crack front, using a surface integral formulation, requires integrations over surfaces of wedge-shaped sectors focussed on the crack front. The accurate evaluation of these integrals appears difficult. In fact, in two-dimensional problems it has been noted that calculation of the J integral is inaccurate for paths traversing the first ring of elements [11], as has also been observed for the virtual crack extension technique. Increasingly, more accurate values are obtained for paths that traverse regions more remote from the crack tip.

From the preceding discussion it is clear that comparison of the area integral (or volume integral) and the line integral (or surface integral) techniques for determining the energy release rate is appropriate. For the present purposes, we confine attention to a solid characterized by a path-independent deformation theory of plasticity.

2. ENERGY RELEASE RATE AND CRACK TIP FIELDS

For a two-dimensional, planar, nonlinear elastic solid, using the small displacement gradient assumption and with body forces neglected, the path-independent J integral is defined by [7]

$$J = \int_\Gamma \left[W n_1 - \sigma_{ij} n_i \frac{\partial u_j}{\partial x_1} \right] ds, \tag{2.1}$$

where, in a cracked body, Γ is any path beginning at the bottom crack face and ending on the top face as shown in Fig. 1. Here, n_i is the outward normal to Γ, σ_{ij} the stress, u_i the displacement, ds the increment of arc length along Γ and W the strain energy density defined by

$$W(\epsilon_{kl}) = \int_0^{\epsilon_{kl}} \sigma_{ij}\, d\epsilon_{ij}. \tag{2.2}$$

Consider a material with the uniaxial stress strain curve represented by

$$\frac{\epsilon}{\epsilon_0} = \alpha \left(\frac{\sigma}{\sigma_0} \right)^n \tag{2.3}$$

for $\epsilon \gg \epsilon_0$, where σ_0 is the yield stress, $\epsilon_0 = \sigma_0/E$ the yield strain, E the elastic modulus, α a material constant and n the strain hardening exponent. For this material, Hutchinson [12] and

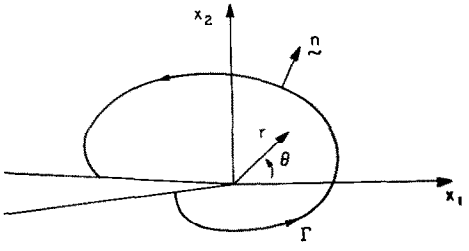

Fig. 1. Crack tip coordinates and contour for the evaluation of the J integral.

Rice Rosengren [13] showed that the asymptotic crack tip fields are

$$\sigma_{ij} = \sigma_0 \left[\frac{J}{\alpha \sigma_0 \epsilon_0 I_n r} \right]^{1/n+1} \tilde{\sigma}_{ij}(\theta, n), \tag{2.4}$$

$$\epsilon_{ij} = \alpha \epsilon_0 \left[\frac{J}{\alpha \sigma_0 \epsilon_0 I_n r} \right]^{n/n+1} \tilde{\epsilon}_{ij}(\theta, n), \tag{2.5}$$

where r and θ are polar coordinates centered at the tip. The dimensionless constant I_n and the dimensionless circumferential variation of $\tilde{\sigma}_{ij}$ and $\tilde{\epsilon}_{ij}$ have been tabulated for Mode I loading under plane strain and plane stress conditions and a wide range of n values [14].

Focussing attention on plane strain, the potential energy per unit thickness π is

$$\pi = \int_A W(\epsilon_{ij})\, dA - \int_{s_T} \bar{T}_i u_i\, ds, \tag{2.6}$$

where s_T is the portion of the boundary where the traction $\bar{T}$ ($\bar{T}_i = \sigma_{ji} n_j$) is prescribed. Let the decrease in π due to a unit advance of crack in its plane (per unit thickness) with tractions held fixed be denoted by $\mathcal{G}$, i.e.

$$\mathcal{G} = -\frac{\partial \pi}{\partial l}\bigg|_{\bar{T}}, \tag{2.7}$$

or

$$\mathcal{G}\, \delta l = -\delta \pi. \tag{2.8}$$

The J integral (2.1) is also the energy release rate [7], i.e.

$$J\, \delta l = -\delta \pi. \tag{2.9}$$

For a plane strain tensile crack, with the crack advancing uniformly through the thickness in its plane, J and $\mathcal{G}$ are equivalent, and we shall use the symbol J to emphasize its definition based on the line integral expression, and $\mathcal{G}$ to emphasize its energy release rate definition.

For a cavity or crack in a three-dimensional body, the J integral generalizes to a surface integral [10], which provides a global energy comparison that does not reveal the variation in the strength of the crack tip fields along the crack front. However, we can appeal to (2.8) for a pointwise definition of energy release rate along the crack front. We consider the planar crack front with a continuously turning tangent. Let $\delta l(s)$ denote the crack advance at the points in the direction normal to the crack front and in the plane of the crack, and let ds denote the elemental arc length along the crack front, as depicted in Fig. 2b. Then, to within first-order terms in δl, $\mathcal{G}(s)$ is defined by the relation [15]

$$\int_{\text{crack front}} \mathcal{G}(s)\, \delta l(s)\, ds = -\delta \pi \tag{2.10}$$

for arbitrary δl.

The interest in determining $\mathcal{G}(s)$ stems from its role as a characterizing parameter of crack tip fields. Consider a crack front with a continuously turning tangent, and focus on a neighborhood of the crack front sufficiently far away from its intersection with the external surface of the body. Let r and θ be the polar coordinates in x_1–x_2 plane, as indicated in Fig. 2. For the planar tensile cracks on which attention is focussed here, it can be argued that the strains tangential to the crack front (ϵ_{i3} in the coordinate system of Fig. 2) remain bounded as $r \to 0$, while the remaining strains become singular. Then, asymptotically, as $r \to 0$, plane strain conditions prevail so that the three-dimensional deformation fields approach the plane strain

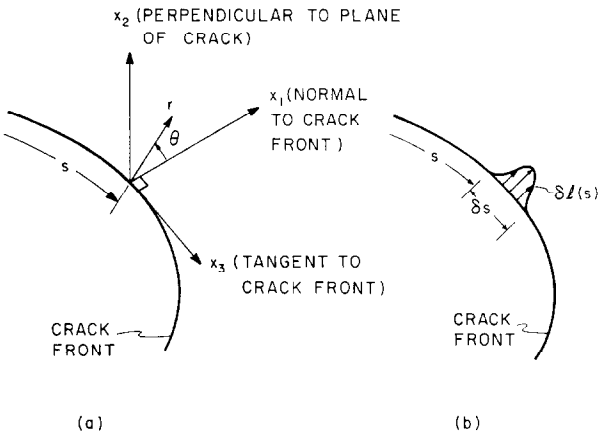

Fig. 2. (a) Definition of local orthogonal Cartesian coordinates at the point s on the crack front. The crack plane is the x_1–x_3 plane. (b) The function $\delta l(s)$ can be pictured as a virtual crack advance in the direction normal to the crack front in the crack plane.

Hutchinson, Rice and Rosengren fields (2.4) and (2.5). The local value of the energy release rate, $\mathcal{G}(s)$, replaces J as an amplitude parameter in (2.4) and (2.5). Although this conclusion is plausible, the argument needs to be made precise and a complete derivation of three-dimensional near tip fields remains to be carried out. An important issue in this regard concerns the size of the region over which any singular field dominates.

3. A VOLUME INTEGRAL EXPRESSION FOR THE ENERGY RELEASE

3.1 *Two-dimensional specialization*

Although the real utility of the volume integral approach lies in applications to three-dimensional crack configurations, the numerical examples to be presented subsequently are restricted to two-dimensional configurations. Here, we briefly describe the two-dimensional area integral analog of the volume integral expression for the energy release rate. We consider an annular region A_I around the crack tip which encloses no other crack or void, as depicted in Fig. 3. First, we write (2.1) in the form

$$\mathcal{G} = J = -\int_{C_1}\left[\sigma_{ij}\frac{\partial u_i}{\partial x_1} - W\,\delta_{1j}\right]n_j\,ds = \int_{C_1} P_{1j}n_j\,ds. \tag{3.1}$$

Here P_{1j} is the x_1 component of Eshelby's [8, 9] energy momentum tensor. The closed curve bounding A_I is denoted by C, and $\mathbf{m}$ is the outward pointing normal on C. Hence, $\mathbf{m} = -\mathbf{n}$ on C_1, and $\mathbf{m} = \mathbf{n}$ on C_2 and the closed curve C in Fig. 3 can be written as $C = C_2 + C_3 - C_1 + C_4$. Since both $\sigma_{ij}\cdot m_j = 0$ and $m_1 = 0$ on C_3 and C_4, we can write (3.1) in the form

$$\mathcal{G}\,\Delta a = \Delta a \oint_C \left[\sigma_{ij}\frac{\partial u_i}{\partial x_1} - W\,\delta_{1j}\right]q_1 m_j\,ds = -\Delta a \oint_C P_{1j}q_1 m_j\,ds, \tag{3.2}$$

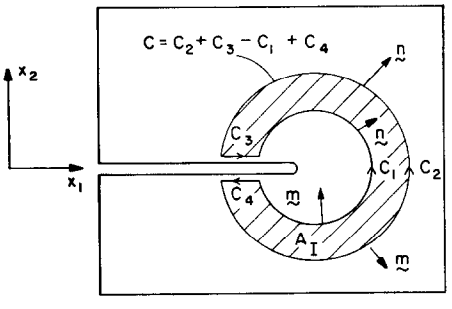

Fig. 3. Simply connected region A_I enclosed by the contour C ($C = C_2 + C_3 - C_1 + C_4$).

where q_1 is a sufficiently smooth function in A_I that is unity on C_1 and vanishes on C_2, and Δa is a scale factor that can be interpreted as an increment of crack advance.

Applying the divergence theorem to (3.2) gives

$$\mathcal{G}\,\Delta a = -\Delta a \int_{A_I} \left[\frac{\partial}{\partial x_j}(P_{1j}q_1)\right] \mathrm{d}A = -\Delta a \int_{A_I} \left[\frac{\partial P_{1j}}{\partial x_j} q_1 + P_{1j}\frac{\partial q_1}{\partial x_j}\right] \mathrm{d}A. \tag{3.3}$$

A direct calculation shows $\partial P_{1j}/\partial x_j = 0$ in A_I [8, 9] [we presume $W = W(\epsilon_{kl})$, with no explicit dependence on x_i], so that (3.3) reduces to the desired area integral expression for $\mathcal{G}$:

$$\mathcal{G} = -\int_{A_I} P_{1j}\frac{\partial q_1}{\partial x_j}\,\mathrm{d}A = \int_{A_I}\left[\sigma_{ij}\frac{\partial u_i}{\partial x_1} - W\,\delta_{1j}\right]\frac{\partial q_1}{\partial x_j}\,\mathrm{d}A. \tag{3.4}$$

The expression (3.4) is consistent with the one obtained by deLorenzi [5, 6], who interpreted $\Delta a\, q_1$ as a mapping function between configurations with slightly differing crack lengths. Here, the equality of the line integral and area integral representations of $\mathcal{G}$, (3.2) and (3.4), follows from a virtual-work-type identity for the x_1 component of Eshelby's [8, 9] energy momentum tensor.

3.2 *Three-dimensional formulation*

We consider an elastic solid with a traction-free portion of the external surface S_t varying with velocity v_j, as illustrated in Fig. 4. The applied loads and prescribed displacements are presumed to remain fixed during this process. The rate of change of the potential energy is given by [10]

$$\frac{\mathrm{d}\pi}{\mathrm{d}t} = \int_{V(t)} \dot{W}\,\mathrm{d}V + \int_{S_t(t)} W v_j m_j\,\mathrm{d}S - \int_{S_T} \bar{T}_i \dot{u}_i\,\mathrm{d}S, \tag{3.5}$$

where $\mathbf{m}$ is the outward pointing normal on S_t, the $\bar{T}_i$ are the prescribed tractions on S_T and $(\dot{}) = \mathrm{d}(\ )/\mathrm{d}t$, t being a monotonically increasing timelike parameter.

Using the principle of virtual work,

$$\int_{V(t)} \dot{W}\,\mathrm{d}V = \int_{V(t)} \sigma_{ij}\dot{\epsilon}_{ij}\,\mathrm{d}V = \int_{S_T} \bar{T}_i \dot{u}_i\,\mathrm{d}S,$$

$\mathrm{d}\pi/\mathrm{d}t$ in (3.5) simplifies to [10]

$$\frac{\mathrm{d}\pi}{\mathrm{d}t} = \int_{S_t(t)} W v_j m_j\,\mathrm{d}S. \tag{3.6}$$

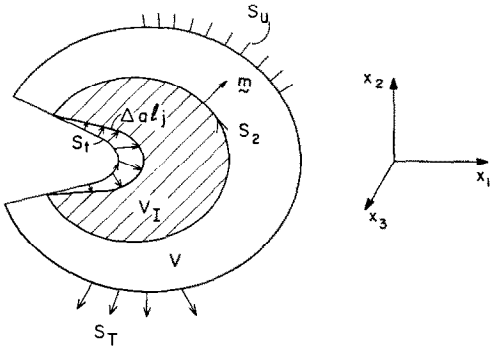

Fig. 4. Schematic of planar section of body containing a notch. The surfaces S_t and S_2 enclose a simply connected volume V_I.

We now presume that along the traction-free surface S_t the notch advances a distance $\Delta a\, l_j$ per unit time in the x_j direction as illustrated in Fig. 4. In general, l_j will vary along S_t. With $v_j = \Delta a\, l_j/\mathrm{d}t$, where l_j can be taken to be in the direction of the normal to S_t at each point, the energy released during notch advance is

$$\bar{\mathcal{G}}\,\Delta a = -\Delta a \int_{S_t(t)} W l_j m_j \,\mathrm{d}S, \tag{3.7}$$

where $\bar{\mathcal{G}}$ is the total energy decrease per unit notch advance.

Since the surface S_t is traction free, eqn (3.7) can be rewritten in the form

$$\bar{\mathcal{G}}\,\Delta a = \Delta a \int_{S_t} \left[\sigma_{ik}\frac{\partial u_i}{\partial x_j} - W\,\delta_{jk}\right] l_j m_k \,\mathrm{d}S = -\Delta a \int_{S_t} P_{jk} l_j m_k \,\mathrm{d}S, \tag{3.8}$$

where P_{jk} is Eshelby's [8, 9] energy momentum tensor. Note that when $\Delta a\, l_j$ corresponds to a translation, l_j can be taken out from the integral sign and (3.8) gives $\bar{\mathcal{G}} = l_j J_j$, where the J_j are the conservation J_j integrals [10].

Let C_I be the curve separating S_t from the remainder of the notch surface, and let S_2 be any surface emanating from C_I and completely surrounding S_t, as illustrated in Fig. 4. It is also presumed that the volume between S_t and S_2 is simply connected.

In order to develop a volume integral expression for the energy released analogous to the one given for the two-dimensional case, we first introduce the functions q_j by

$$q_j = \begin{cases} l_j & \text{on } S_t, \\ 0 & \text{on } S_2, \end{cases} \tag{3.9}$$

together with the requirement that q_j be sufficiently smooth in the volume enclosed by S_t and S_2.

Using (3.8) and (3.9), the energy released when the notch advances $\Delta a\, l_j$ can be written as

$$\bar{\mathcal{G}}\,\Delta a = \Delta a \int_{S_t - S_2} \left[\sigma_{ik}\frac{\partial u_i}{\partial x_j} - W\,\delta_{kj}\right] q_j m_k \,\mathrm{d}S = -\Delta a \int_{S_t - S_2} P_{jk} q_j m_k \,\mathrm{d}S. \tag{3.10}$$

We now focus attention on a notch, as depicted in Fig. 5, where the notch thickness is denoted by h. Ultimately, we will pass (heuristically) to the limiting case of the notch becoming a sharp crack, i.e. $h \to 0$. The surface of the notch consists of faces with normals along x_2, S_A and S_B, and a face with a normal in the x_1–x_3 plane, S_t. We restrict l_j to lie along S_t and to be a function of x_1 and x_3 only. For this special case l_2 and q_2 in (3.9) vanish identically. The path of integration is taken along some surface surrounding the notch front and not enclosing any other notch or void, such as the path $S = S_2 + S_3 - S_t + S_4$ in Fig. 5. Since the traction vanishes on the crack faces and both $m_1 = 0$ and $m_3 = 0$ along S_3 and S_4, the integrand in (3.10) vanishes along these surfaces. Hence, for S

$$\bar{\mathcal{G}} = -\oint_S P_{jk} q_j m_k \,\mathrm{d}S. \tag{3.11}$$

The distinction between (3.11) and (3.10) lies in the more general paths allowed owing to the special notch geometry; i.e. the path S_2 in (3.11) may intersect the notch surface anywhere along the upper and lower faces, S_A and S_B, in Fig. 5.

As in (3.3), applying the divergence theorem and making use of the relation $\partial P_{ij}/\partial x_j = 0$ give the result [5]

$$\bar{\mathcal{G}} = -\int_{V_t} P_{jk}\frac{\partial q_j}{\partial x_k}\,\mathrm{d}V = \int_{V_t}\left[\sigma_{ik}\frac{\partial u_i}{\partial x_j} - W\,\delta_{kj}\right]\frac{\partial q_j}{\partial x_k}\,\mathrm{d}V. \tag{3.12}$$

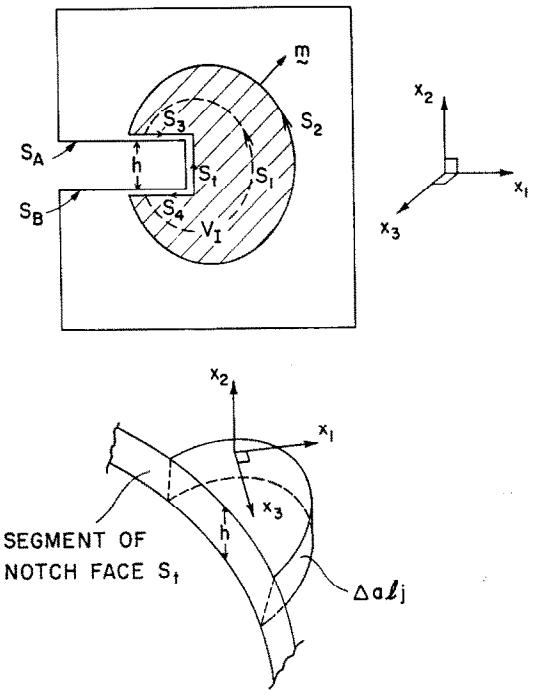

Fig. 5. (a) Schematic of section of body in the x_1–x_2 plane containing a notch of thickness h. (b) Schematic of notch face where the function $\Delta a\, l_j$ is interpreted as a virtual advance of a segment of the notch face in the direction normal to x_2; note that l_2 vanishes identically.

We now let $h \to 0$ to obtain the desired expression for the energy decrease when a portion of a surface crack front advances by $\Delta a\, l_j$ in its plane.

We note that the equality of (3.11) and (3.12) holds for any arbitrary (sufficiently smooth) function q_j. For example, if q_j is independent of position in V_I, the gradient in (3.12) vanishes, expressing the fact that the J_j integrals vanish around closed contours enclosing simply connected regions. In particular, when l_j in Fig. 5 corresponds to a translation, we can shift the region of integration away from the crack tip. First, we let $q_j = l_j$, where each l_j is a constant, in the region between S_t and S_1. Then, invoking path independence of the J_j integrals [or, equivalently, from (3.11) and (3.12)], we can replace the path along S_t by the path along S_1 in (3.9)–(3.11). The volume of integration in (3.12) then becomes the region between S_1 and S_2 in Fig. 5. In the two-dimensional case depicted in Fig. 3, attention is confined to a crack translation from the outset, and the integration is carried out over the annular region between C_1 and C_2. Although there are path-independent integrals for other choices of the l_j [10], in general, the computation of the energy decrease for l_j varying along the crack front requires integration over the surface S_t or the volume between S_t and S_2 in Fig. 5.

4. FINITE-ELEMENT FORMULATION FOR THE VOLUME INTEGRAL METHOD

4.1 *Two-dimensional specialization*

We discuss the implementation of the area integral expression (3.4) within the context of the displacement finite-element method and in conjunction with the biquadratic (Lagrangian) shape functions. In isoparametric (η_1, η_2) $(-1 \le \eta_i \le 1,\ i = 1, 2)$ space, the shape functions are constructed from the basic functions

$$f_1 = -\tfrac{1}{2}\eta(1-\eta), \quad f_2 = (1-\eta)(1+\eta), \quad f_3 = \tfrac{1}{2}\eta(1+\eta) \tag{4.1}$$

via

$$N_{3J+I-3} = f_I(\eta_1) f_J(\eta_2), \quad I, J = 1, 2, 3 \tag{4.2}$$

Then the coordinates (x_1, x_2) in the physical space and the displacements (u_1, u_2) are written as

$$x_i = \sum_{K=1}^{9} N_K X_{iK}, \quad u_i = \sum_{K=1}^{9} N_K U_{iK}, \quad i = 1, 2, \tag{4.3}$$

where the X_{iK} are the nodal coordinates and the U_{iK} the nodal displacements.

In finite-element analyses, the area A_I in (3.4) is partitioned into elements. Consistent with the isoparmetric formulation, we take q_1 within an element as

$$q_1 = \sum_{I=1}^{9} N_I Q_{1I}, \tag{4.4}$$

where Q_{1I} are the nodal values for the Ith node. From the definition of q_1, if the Ith node is on C_1, $Q_{1I} = 1$, whereas if the Ith node is on C_2, $Q_{1I} = 0$. In the area between C_1 and C_2, Q_{1I} will be taken to vary between 0 and 1. Using (4.3), (4.4) and the chain rule for partial derivatives, the spatial gradient of q_1 within an element is given by

$$\frac{\partial q_1}{\partial x_j} = \sum_{I=1}^{9} \sum_{J=1}^{2} \frac{\partial N_I}{\partial \eta_J} \frac{\partial \eta_J}{\partial x_j} Q_{1I}, \tag{4.5}$$

where $\partial \eta_J / \partial x_j$ is the inverse Jacobian matrix of the transformation (4.3). With 3×3 Gaussian integration, the discretized form of the area integral expression for the energy release rate (3.4) is

$$\mathcal{G} = \sum_{\substack{\text{elements} \\ \text{in } A_I}} \sum_{p=1}^{9} \left[\left(\sigma_{ij} \frac{\partial u_i}{\partial x_1} - W \delta_{1j} \right) \frac{\partial q_1}{\partial x_j} \det \left(\frac{\partial x_K}{\partial \eta_K} \right) \right]_p w_p. \tag{4.6}$$

Here the quantities within $[\ \ ]_p$ are evaluated at the nine Gauss points, and w_p are the respective weights. In the case in which selective/reduced integration (3×3 and 2×2 integration for deviatoric and volumetric terms, respectively) is employed in the formation of the stiffness matrix, the bracketed quantities are decomposed into deviatoric and volumetric parts (see Ref. [11]),

$$\mathcal{G} = \sum_{\substack{\text{elements} \\ \text{in } A_I}} \left\{ \sum_{p=1}^{9} \left[\begin{matrix} \text{deviatoric} \\ \text{terms} \end{matrix} \right]_p w_p + \sum_{p=1}^{4} \left[\begin{matrix} \text{volumetric} \\ \text{terms} \end{matrix} \right]_p w_p \right\}. \tag{4.7}$$

The function q_1 can be interpreted as imposing on the material points within C_1 a unit translation in the x_1 direction, while requiring the material points on C_2 to remain fixed. The material points within A_I (area bounded by C_1 and C_2) are displaced according to (4.4). Thus, the area integral method can be interpreted as a virtual crack extension technique. As discussed in Section 3, the contours C_1 and C_2 are nonintersecting paths beginning at the bottom crack face and ending on the top face. By letting C_1 and C_2 coincide with the boundaries of different rings of elements, including the possibility of C_1 shrinking onto the crack tip, the energy release rate $\mathcal{G}$ can be evaluated on alternate paths, as illustrated in Fig. 6. In this respect we note that the nodal values Q_{1I} within A_I can be arbitrarily chosen as long as they are compatible with the prescribed values on C_1 and C_2. We employed a practical scheme so that for a node inside A_I, Q_{1I} is given by linear interpolation with respect to its associated boundary nodes on C_1 and C_2. This is schematically depicted in Fig. 6. Other interpolation schemes can also be adopted for this purpose. We note that a particular choice of interpolation scheme for Q_{1I} is equivalent to selecting a particular weighting scheme for the field quantities between C_1 and C_2.

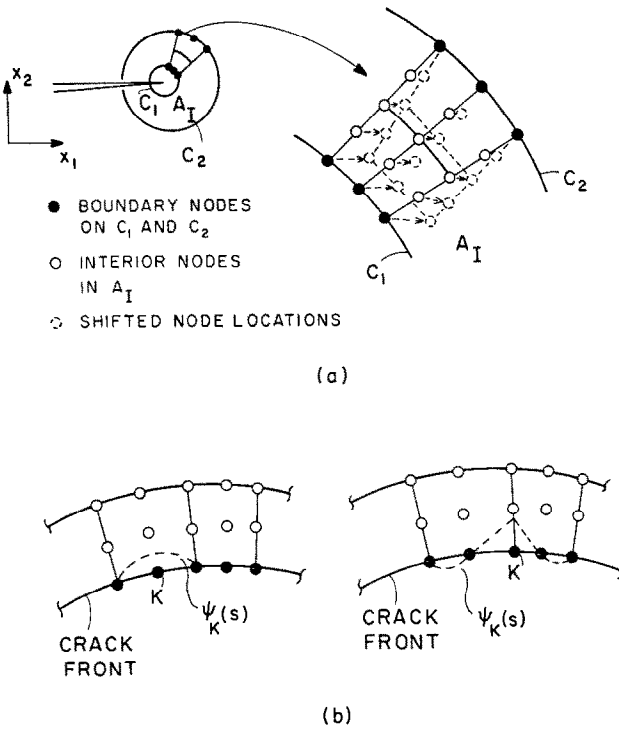

Fig. 6. (a) Schematic of finite-element mesh in the x_1–x_2 plane where the function q_1 is interpreted as imposing a translation on the nodes in the x_1 direction. This figure depicts the 2-D case. For the case of the 3-D crack, the crack front S_t and the surface S_2 replace C_1 (C_1 is shrunk onto the crack tip) and C_2, respectively. The schematic then represents a planar section of the volume V_I^M. (b) Basis functions $\psi_K(s)$ for "midnodes" and "corner nodes."

4.2 *Three-dimensional formulation*

We present the finite-element implementation of the three-dimensional expression (3.12) for the triquadratic (Lagrangian) shape functions. The expression analogous to (3.9) which is consistent with the isoparametric formulation is

$$q_i = \sum_{I=1}^{27} N_I Q_{iI}. \tag{4.8}$$

Here, N_I is the triquadratic Lagrangian shape function, and the Q_{iI} are the nodal values for the Ith node. As discussed in the two-dimensional specialization of this method, $Q_{iI} = 0$ if the Ith node is on S_2 (see Fig. 5). For nodes lying within V_I, Q_{iI} is given by interpolating between the associated boundary nodes on S_t and S_2. Furthermore, for the cases of interest here, it is noted that Q_{2I} vanishes identically. Following standard manipulations described in the two-dimensional derivation,

$$\frac{\partial q_i}{\partial x_j} = \sum_{I=1}^{27} \sum_{J=1}^{3} \frac{\partial N_I}{\partial \eta_J} \frac{\partial \eta_J}{\partial x_j} Q_{iI}. \tag{4.9}$$

Employing 3 × 3 × 3 Gaussian integration, the discretized form for (3.12) is

$$\overline{\mathcal{G}} = \sum_{\substack{\text{elements} \\ \text{in } V_I}} \sum_{p=1}^{27} \left[\left(\sigma_{ik} \frac{\partial u_i}{\partial x_j} - W \delta_{kj} \right) \frac{\partial q_j}{\partial x_k} \det \left(\frac{\partial x_K}{\partial \eta_K} \right) \right]_p w_p. \tag{4.10}$$

Here the quantities within $[\ ]_p$ are evaluated at the 27 Gauss points, and w_p are the respective weights. If selective/reduced integration is employed in the formation of the stiffness matrix, then an expression similar to (4.7) is applicable.

The relation between the energy released for a virtual advance over a finite segment of the crack and the pointwise energy release rate $\mathcal{G}(s)$ is given by (2.11), which we rewrite in the form

$$\Delta a \int_{\text{crack front}} \mathcal{G}(s) l_j(s) m_j \, ds = \overline{\mathcal{G}} \, \Delta a. \tag{4.11}$$

As can be seen in (4.11), $\overline{\mathcal{G}}$ has dimensions energy over length, whereas $\mathcal{G}(s)$ has dimensions energy over area. In the special case of a plane strain tensile crack advancing uniformly along its front so that $\mathcal{G}(s)$ is constant along the crack front, $\overline{\mathcal{G}}$ divided by the length of crack front is the constant value of $\mathcal{G}(s)$. It is this value that has been denoted $\mathcal{G}$ in our discussion of plane strain tensile cracks.

We restrict our attention to the case of a planar crack front with a continuously turning tangent and assume that $\mathcal{G}(s)$ is a sufficiently smooth function of s. Let $\mathcal{G}_K$ denote the value of $\mathcal{G}(s)$ at the Kth node on the crack front, and $\psi_K(s)$ be any suitable piecewise basis functions defined along the crack front where

$$\psi_K = \begin{cases} 1 & \text{at the } K\text{th node,} \\ 0 & \text{at all other nodes.} \end{cases} \tag{4.12}$$

We represent $\mathcal{G}(s)$ by

$$\mathcal{G}(s) = \sum_{K=1}^{N} \mathcal{G}_K \psi_K(s), \tag{4.13}$$

where N is the number of nodes on the crack front. Similarly, the function $l_j m_j$ in (4.11) can be represented in terms of the same basis functions:

$$l_j(s) m_j(s) = \sum_{J=1}^{N} L_J \psi_J(s), \tag{4.14}$$

where L_J is the prescribed nodal value for the Jth node on the crack front.

We direct our attention to a particular node M on the crack front and make the choice

$$L_J^M = \begin{cases} 1, & J = M, \\ 0, & J \neq M, \end{cases} \qquad 1 \leq J \leq N. \tag{4.15}$$

Let V_I^M denote the volume of the elements with nonvanishing q_i. This volume must contain node M as a member node. For this particular choice of L_J, q_i in V_I^M is given by (4.8), with Q_{iI} replaced by Q_{iI}^M, where we take

$$Q_{iI}^M = m_i^M, \quad I = M, \tag{4.16}$$

and m_i^M is the normal to the crack front (in the x_1–x_3 plane of Fig. 5) at the node M. At other nodes, the nodal values Q_{iI}^M are obtained by interpolation, subject to the restriction that the nodal values on S_t (except for node M) and on S_2 are zero. A particular choice of interpolation of the nodal values Q_{iI}^M implicitly picks a weighting function for evaluating the integral (4.10) and defines the volume V_I^M. Explicitly, V_I^M is the volume over which q_i in (4.8) does not vanish identically. The choice of nodal values is subect to considerations of numerical accuracy, as well as computational convenience.

We evaluate $\overline{\mathcal{G}}$ for the particular choice of L_J by substituting (4.9), with the appropriate Q_{iI}^M, into (4.10) and carrying out the integration as indicated; it may be noted that the outer

summation need only include the elements in V_I^M. The results can be written as

$$\overline{\mathcal{G}} = \sum_{I=1}^{U} \sum_{i=1}^{3} B_{iI} Q_{iI}^M, \tag{4.17}$$

where U is the number of nodes in V_I^M, and B_{iI} are the contributions from the field quantities associated with the Ith node in V_I^M, where here $Q_{2I}^M \equiv 0$.

To obtain an explicit expression for $\mathcal{G}_K$, we substitute (4.13) and (4.14) into the left-hand side of (4.11) to get

$$\overline{\mathcal{G}} = \sum_{K=1}^{N} \mathcal{G}_K \int_{S_t} \psi_M(s)\psi_K(s)\, \mathrm{d}s. \tag{4.18}$$

Here the integration need only be carried out over the part of the crack front where the basis function $\psi_M(s)$ is nonzero. The resulting expression can be written as

$$\overline{\mathcal{G}} = \sum_{K=1}^{N} A_{MK} \mathcal{G}_K, \tag{4.19}$$

where A_{MK} is the coefficient for the Kth node and is nonzero only for nodes on the crack front of V_I^M. Equating the expressions for $\overline{\mathcal{G}}$ in (4.17) and (4.19), we have an equation which is linear in the unknowns $\mathcal{G}_K$ given by

$$\sum_{K=1}^{N} A_{MK} \mathcal{G}_K = \sum_{I=1}^{U} \sum_{i=1}^{3} B_{iI} Q_{iI}^M. \tag{4.20}$$

By repeating the above process for every node on the crack front, we obtain a linear system of N equations with N unknown $\mathcal{G}_K$. The pointwise energy release rate is given by substituting the solution for $\mathcal{G}_K$ into (4.13).

We remarked earlier that $\psi_K(s)$ in (4.13) and (4.14) can be any suitable basis functions. An obvious choice here is to let $\psi_K(s)$ be given by the Lagrangian quadratic basis function for the Kth node. For this particular choice, the basis functions and the interval over which they are nonzero are depicted in Fig. 6, and, as a consequence, the bandwidth of A_{MK} is 5.

5. ELASTIC AND FULLY PLASTIC CRACK ANALYSES

5.1 *Fully plastic formulation*

The plane strain edge-cracked panel (ECP) subject to remote loading, as shown in Fig. 7, is the model configuration for our studies. Here, the statically equivalent tensile load and moment (per unit thickness) acting on the panel are denoted by P and M, and a and b are the crack length and width, respectively. It is convenient to introduce the dimensionless load parameter λ defined by

$$\lambda = \frac{M}{Pb}, \tag{5.1}$$

where $\lambda = 0$ and $\lambda \to \infty$ correspond to only tensile load and moment, respectively, being applied at the remote ends. We employ the pure power constitutive relation (2.3), also referred to as the fully plastic material, with a slightly modified form of (2.3) invoked within the Newton–Raphson iterative process to ensure uniform quadratic convergence. The generalization of (2.3) to multiaxial stress states according to J_2 deformation plasticity theory, the finite-element penalty formulation for incompressible plane strain deformation and the details of its implementation for a nine-noded biquadratic (Lagrangian) element are discussed in Ref. [11]. Solutions

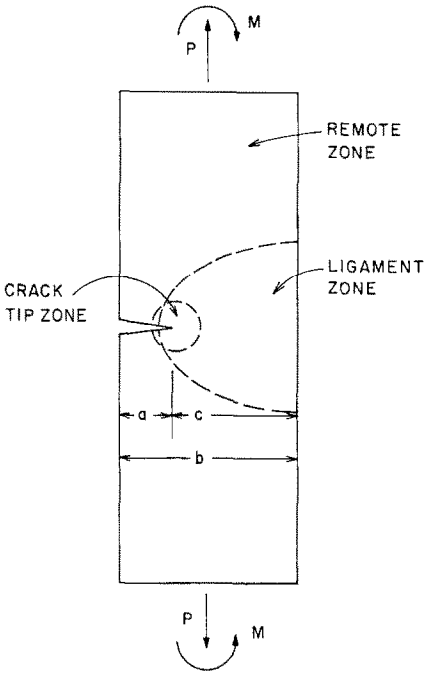

Fig. 7. Edge-cracked panel subject to remote tension and bending.

to such formulations, frequently referred to as fully plastic solutions, possess scaling properties which are useful in nonlinear fracture analysis. In addition, the energy release rate and the work conjugate displacements satisfy certain consistency relations, which can be used as a check on the consistency of numerical solutions.

5.2 *Finite-element mesh*

The ECP with a crack-length-to-width ratio, a/b, of $\frac{1}{4}$ was chosen for our studies. The mesh we generate has three distinct zones, namely, the near-tip, ligament and remote zones. The near-tip zone consists of several layers of circular rings of elements which are centered about the crack tip. The first ring consists of wedge-shaped elements; i.e. one edge of the element is shrunk onto a point which coincides with the crack tip location. Hence, each element has three nodes at the crack tip location. This ring of elements is called the crack tip ring.

In an elastic analysis ($n = 1$), the nodes at the crack tip are tied together, and therefore the crack tip displaces as a single node. Two variations are possible. If the midedge nodes and the interior node are placed at their usual midpositions, the crack tip element is a conventional wedge element and the displacement gradients are nonsingular. If the nodes along the radial edges and the interior node are placed at the appropriate quarter positions, the element is called the singular elastic wedge element and the displacement gradients contain terms of order $(1/\sqrt{r})$, which is consistent with continuum crack tip fields for elastic bodies. An appropriate element for plasticity analysis is the singular plastic wedge element, where the three nodes at the crack tip can displace independently, while the midedge nodes and the interior node are placed at their usual midpositions. Displacement gradients associated with this element contain terms of order $(1/r)$, which is consistent with the continuum crack tip fields for elastic–perfectly plastic bodies [16]. Nevertheless, finite-element studies show that this element can also be used for strain hardening solids [11]. The crack tip ring of elements and the conventional and singular wedge elements are schematically depicted in Fig. 8.

Within the ligament zone, the mesh is designed to accommodate deformation patterns similar to the fully plastic slip line field relevant to this cracked configuration. Previous studies have shown that the use of the appropriate elements in the crack tip zone and proper mesh design in the ligament zone are essential for accurate solutions [17]. The meshes for the upper half of the ECP are shown in Fig. 9.

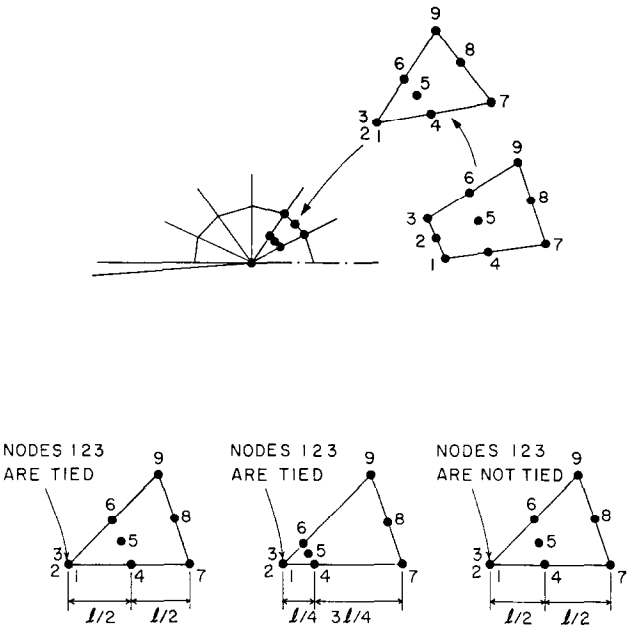

Fig. 8. Sketch of assembly of wedge-shaped elements that surround upper half of crack tip. The elastic-wedge element, singular elastic-wedge element and singular plastic-wedge element are illustrated.

5.3 *Parameter tracking procedure*

The Newton–Raphson method converges if the initial estimate of the solution is sufficiently close to the actual solution. Our solution procedure begins with obtaining the solution to the linear problem ($n = 1$) for a particular remote load combination (say $\lambda = 0$). As in a previous study [11], a parameter tracking procedure is employed to generate solutions for various values of n and λ. Here, for a given strain hardening exponent n, the solutions for a particular load combination, say $\lambda = 0$, are employed as initial estimates for another series of calculations for a slightly different load combination. For example, the $n = 5$ and 10 solutions for $\lambda = 0$ can be used as the initial estimates of the $n = 5$ and 10 solutions for $\lambda = -\frac{1}{16}$. In this case, λ serves as the tracking parameter. Solutions for $n = 1, 2, 3, 5, 7$ and 10 and $\lambda = 0$ and $-\frac{1}{16}$ were thus obtained. In this paper only the results for $n = 1, 5$ and 10 are discussed.

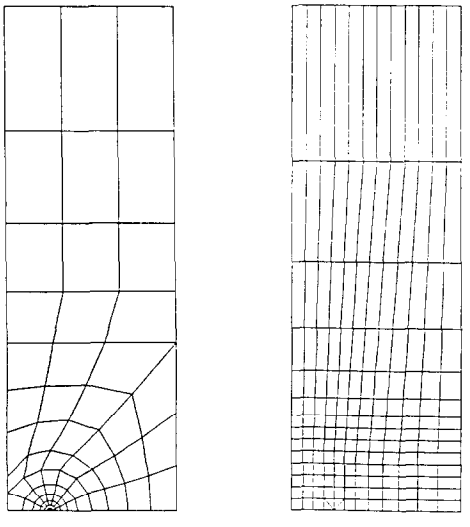

Fig. 9. 78-element and 170-element models for the upper half of the edge-cracked panel.

5.4 *Comparison of area integral and line integral methods*

Convergent solutions were obtained for $n = 1$, 5 and 10, and $\lambda = 0$ and $\lambda = -\frac{1}{16}$ with the 78-element model shown in Fig. 9. In one series of calculations the crack tip ring of the element was formed by conventional wedge elements, which are nonsingular. The calculations were repeated with singular elastic-wedge elements for the elastic problem ($n = 1$) and singular plastic-wedge elements for the nonlinear elastic problems ($n > 1$). These finite-element solutions were postprocessed by the area integral routines, which were implemented along the lines described in Section 4, and the line integral routines developed in an earlier study [11].

The values of $\mathcal{G}$ determined from the two methods using finite-element solutions obtained with the use of the singular crack tip ring of elements are tabulated in Table 1. Path 1 denotes the path through the crack tip ring of elements, Path 2 passes through the next ring of elements and so on. Path 10 passes through elements on the remote edges of the panel. We examine the $\mathcal{G}$ values determined by the line integral method first. In the elastic case, the various path values (including the crack tip value) differ by about 2%. For $n = 5$ and 10 the values determined from Path 2 to 10 are in good agreement. However, the crack tip values deviated from the "consensus" or mean values by 5 to 10%. For comparison purposes the mean value from an earlier analysis, which uses a rather different mesh design, is also included in the table. Next, we examine the values of $\mathcal{G}$ determined by the area integral method. Here the values for *all* rings and *all* the n's considered are essentially path independent. This degree of path independence was also observed in the calculations we carried out for a wide range of λ's and a/b ratios. These results will be reported in a separate paper.

For the purpose of quantifying the comparison between the two methods, the mean value of $\mathcal{G}$ for a particular solution is computed from values associated with paths/rings 2–10. The error for a particular solution is defined by dividing the difference between the crack tip value and the mean value by the mean value. The errors thus defined are tabulated in Table 2 under analyses I, II, III and IV which were carried out for two values of λ with the 78-element model. It is clear that the area integral method is superior to the line integral method. It is also apparent that solutions obtained with nonsingular crack tip elements are not so accurate as solutions obtained with singular crack tip elements. For the latter solutions, we note that the errors for $n = 10$ are smaller than the errors for $n = 5$. This trend is not unexpected, since it is known from the continuum results (2.4, 2.5) that the displacement gradients for $n = 10$ are nearly of order $(1/r)$. Our results suggest that the combination of the appropriate singular crack tip elements and the area integral method is optimum for the determination of $\mathcal{G}$ (and J).

5.5 *Effect of overall mesh design on accuracy*

In a preceding study on mesh design, we showed that mesh refinement within the vicinity of the relevant slip line field is essential for accurate solutions [17]. Here we evaluate two rather different mesh designs which satisfy the above requirement. In this preliminary study we enquire

Table 1. The values of $\mathcal{G}$ evaluated on different rings by line integral and area integral methods from finite-element solutions for $\lambda = 0$

	Path/Rings											
n	1	2	3	4	5	6	7	8	9	10	Mean value	Mean value [11]
Line integral method												
1	97.15	99.97	98.53	98.08	97.89	97.95	95.92	96.04	96.83	97.8	97.32	97.81
5	881.9	828.9	818.5	817.3	821.1	814.8	812.3	810.8	811.1	827.8	815.1	820.4
10	2419	2329	2311	2310	2320	2305	2294	2283	2277	2334	2300	2316
Area integral method												
1	97.13	96.97	97.03	97.03	97.02	97.01	97.07	97.10	97.03	97.03	97.04	
5	803.6	808.8	810.1	810.2	810.1	810.2	810.3	810.7	810.4	811.3	810.3	
10	2290	2294	2295	2294	2293	2293	2297	2297	2296	2289	2295	

Note: The crack tip ring of elements is formed from singular elastic-wedge elements for $n = 1$ and from singular plastic-wedge elements for $n = 5$ and 10.

Table 2. Differernce in percent between $\mathcal{G}$ evaluated on crack tip ring and its mean value: a comparison of two methods, crack tip elements and overall mesh design

Analysis	Methods and Models	λ	$n = 1$	$n = 5$	$n = 10$
I	Line integral method	0	27.92	14.22	8.45
	Nonsingular crack tip element	−1/16	27.44	13.89	8.20
	78-element model				
II	Line integral method	0	0.13	8.20	5.17
	Singular crack tip element	−1/16	0.15	8.81	5.93
	78-element model				
III	Area integral method	0	3.79	10.02	13.00
	Nonsingular crack tip element	−1/16	3.78	10.21	13.23
	78-element model				
IV	Area integral method	0	0.09	0.83	0.21
	Singular crack tip element	−1/16	0.10	0.66	0.006
	78-element model				
V	Area integral method	0	0.24	1.49	0.92
	Singular crack tip element	−1/16	0.29	2.00	1.84
	170-element model				

Note: The nonsingular crack tip element is the conventional wedge element. The singular crack tip elements for $n = 1$, 5 and 10 are the singular elastic- and singular plastic-wedge elements, respectively.

whether there is an optimum orientation and arrangement of elements. To this end, we compare the solutions from two finite-element models shown in Fig. 9. Both models employ the appropriate singular crack tip elements, and $\mathcal{G}$ is determined by the area integral method. Adopting the error definition given in the preceding subsection, we give the results for the 170-element model in Table 2 under Analysis V. Comparing the results grouped under IV and V shows that the crack tip values determined from the 78-element model are more accurate. This is expected, since the 78-element model has seven singular elements within the crack tip ring, whereas the 170-element model has only four singular elements.

A useful normalization for $\mathcal{G}$ (and J) solutions generated for an edge-cracked panel subject to predominantly remote tension is

$$\mathcal{G} \equiv J = \alpha\sigma_0\epsilon_0 \left(\frac{ac}{b}\right) h_1\left(\frac{a}{b}, n, \lambda\right) \left(\frac{P}{P_0}\right)^{n+1}. \tag{5.2}$$

Here P_0 is a reference load, and the dimensionless function h_1 depends on a/b, n and λ; reasons for this normalization are given in Ref. [11]. The normalized values determined from both models and some earlier results are tabulated in Table 3. It is apparent that we were able to obtain the same level of accuracy with the smaller model through an optimum arrangement and orientation of elements. In this regard, we note that the 170-element model requires 3.6 CPU minutes on the VAX 11/780 per iteration of the Newton–Raphson method, whereas the 78-element model requires 1.2 CPU minutes per iteration.

Table 3. Comparison of normalized $\mathcal{G}(J)$ values, h_1, determined from three different meshes

	λ	$n = 1$	$n = 5$	$n = 10$
78-element model	0	4.35	4.45	2.98
Crack tip value	−1/16	2.30	2.12	1.38
78-element model	0	4.34	4.48	2.99
Mean value	−1/16	2.30	2.13	1.38
170-element model	0	4.25	4.45	2.98
Crack tip value	−1/16	2.25	2.11	1.36
170-element model	0	4.26	4.52	3.01
Mean value	−1/16	2.26	2.15	1.39
226-element model Mean value (from [11])	0	4.42	4.54	3.02

6. CONCLUDING REMARKS

We have carried out a comparison of area integral and line integral methods for calculating the energy released during quasi-static crack advancement. A concise derivation of the volume (area) integral expression is obtained using a virtual-work-type identity for Eshelby's [8, 9] energy momentum tensor. The resulting integral is identical to the one deLorenzi [5] derived by direct calculation of the energy difference between configurations with slightly different crack lengths. As noted by deLorenzi [5] (see also Parks [1, appendix]), this volume integral method corresponds to a continuum formulation of the finite-element virtual crack extension technique [1–4]. The three-dimensional analog of the volume integral method appears to be an attractive approach for obtaining pointwise values of the energy release rate along a crack front.

The computational implementation of the method has been outlined for both two- and three-dimensional crack configurations. Numerical results for a fully plastic analysis of a plane strain edge-cracked panel subject to combined bending and tension illustrate the effectiveness of the method. The results also point out the importance of element choice and mesh design for the class of problems considered here. These considerations are of particular relevance to the three-dimensional case for which obtaining pointwise values of the energy release rate along the crack front requires accurate near-tip field quantities.

We have confined attention to cases in which Eshelby's energy momentum tensor [8, 9] satisfies the "homogeneous equilibrium equation" $\partial P_{kj}/\partial x_j = 0$. In more general circumstances, for example, if the material is inhomogeneous (W depends explicitly on position), "body-force"-type terms appear in the equilibrium equation for P_{kj}, and the volume integral expression can be modified to incorporate such terms.

We have also focussed on solids characterized by a path-independent deformation theory of plasticity. The volume integral method can also be employed in crack analyses, when the solid is characterized by an incremental theory of plasticity, if the strain energy density W is replaced by

$$W' = \int_0^{\epsilon_{kl}} \sigma_{kl}\, d\epsilon_{kl},$$

where the integration follows the actual strain trajectory of a material point. For incremental plasticity the interpretation of J [or $\mathcal{G}(s)$] as the energy available to advance the crack cannot be made. However, in circumstances which remain to be fully delineated, J retains significance as a characterizing parameter for crack tip fields [18].

Acknowledgements—The authors are pleased to acknowledge helpful discussions with Professor L. B. Freund of Brown University. F. Z. Li is grateful for support from the Materials Research Laboratory at Brown University, funded by the National Science Foundation. C. F. Shih and A. Needleman gratefully acknowledge the support of the U.S. Department of Energy through grant DE-AC02-80-ER10556. The computations reported on here were carried out on a VAX-11/780 computer at Brown University, Division of Engineering, Computational Mechanics Computer Facility. This facility was made possible by grants from the U.S. National Science Foundation (grant ENG78-19378), the General Electric Foundation and the Digital Equipment Corporation.

REFERENCES

[1] D. M. Parks, A stiffness derivative finite element technique for determination of crack tip stress intensity factors. *Int. J. Fracture* **10**, 487–502 (1974).
[2] D. M. Parks, The virtual crack extension method for nonlinear material behavior. *Comp. Meth. Appl. Mech. Engng* **12**, 353–364 (1977).
[3] D. M. Parks, Virtual crack extensions: A general finite element technique for J-integral evaluation, in *Numerical Methods in Fracture Mechanics* (Edited by A. R. Luxmore and D. R. J. Owen). University College of Wales, Swansea, pp. 464–478 (1978).
[4] T. K. Hellen, On the method of virtual crack extension. *Int. J. Numer. Meth. Engng* **9**, 187–207 (1975).
[5] H. G. deLorenzi, On the energy release rate and the J-integral for 3-D crack configurations. *Int. J. Fracture* **19**, 183–193 (1982).
[6] H. G. deLorenzi, Energy release rate calculations by the finite element method. General Electric Company TIS *Rep. 82CRD205* (1982).
[7] J. R. Rice, A path independent integral and the approximate analysis of strain concentration by notches and cracks. *J. Appl. Mech.* **35**, 379–386 (1968).
[8] J. D. Eshelby, The continuum theory of lattice defects, in *Solid State Physics* (Edited by F. Seitz and D. Turnbull) Vol. III, pp. 79–144. Academic Press, New York (1956).

[9] J. D. Eshelby, The energy momentum tensor in continuum mechanics, in *Inelastic Behavior of Solids* (Edited by M. F. Kanninen *et al.*), pp. 77–114. McGraw-Hill, New York (1970).
[10] B. Budiansky and J. R. Rice, *Conservation laws and energy release rates. J. Appl. Mech.* **40,** 201–203 (1973).
[11] C. F. Shih and A. Needleman, Fully plastic crack problems—Part I: Solutions by a penalty method. *J. Appl. Mech.*, **51,** 48–56 (1984).
[12] J. W. Hutchinson, Singular behavior at the end of a tensile crack in a hardening material. *J. Mech. Phys. Solids* **16,** 13–31 (1968).
[13] J. R. Rice and G. F. Rosengren, Plane strain deformation near a crack tip in a power law hardening material. *J. Mech. Phys. Solids* **16,** 1–12 (1968).
[14] C. F. Shih, Tables of Hutchinson–Rice–Rosengren singular field quantities. Brown University Materials Research Laboratory *Rep. MRL E-147* (1983).
[15] J. R. Rice, P. C. Paris and J. G. Merkle, Some further results on *J*-integral analysis and estimates. Progress in flaw growth and fracture toughness testing, *ASTM STP* 536, 231–245 (1973).
[16] R. S. Barsoum, Triangular quarter-point elements as elastic and perfectly-plastic crack tip elements. *Int. J. Numer Meth. Engng* **11,** 85–98 (1977).
[17] C. F. Shih and A. Needleman, Fully plastic crack problems—Part II: Application of consistency checks. *J. Appl. Mech.*, **51,** 57–64 (1984).
[18] J. W. Hutchinson, Fundamentals of the phenomenological theory of nonlinear fracture mechanics. *J. Appl. Mech.* **50,** 1042–1051 (1983).

(*Received* 23 *February* 1984; *received for publication* 20 *October* 1984)